Flood Susceptibility Mapping using GIS and Evidential Belief Function Model in Lam Chiang Krai Watershed, Nakhon Ratchasima Province, Thailand

Phetprayoon, T.
Geography and Geoinformatics Program, Faculty of Science and Technology, Nakhon Ratchasima Rajabhat University, Nakhon Ratchasima, 30000, Thailand
E-mail: tharapong.p@nrru.ac.th
DOI: https://doi.org/10.52939/ijg.v21i6.4231

Abstract
Flood events are recognized as highly impactful natural hazards, frequently resulting in considerable economic losses across ecosystems, agriculture, and infrastructure. Identifying areas most susceptible to flooding has become a crucial component of flood mitigation plans. The objective of this study is the application of Geographic Information Systems (GIS) integrated with the Evidential Belief Function (EBF) model to flood susceptibility mapping in the Lam Chiang Krai watershed, Nakhon Ratchasima province, Thailand. A flood inventory map was initially generated, and the data were subsequently partitioned into a training dataset (70%) and a validation dataset (30%) for model development and accuracy assessment. Ten flood conditioning factors, such as elevation, slope, curvature, stream power index (SPI), topographic wetness index (TWI), distance to stream, geology, soil texture, land use and land cover (LULC), and mean annual rainfall, were used as thematic layers in the analysis. The potential redundancy among these variables was examined using multicollinearity analysis. An analysis of the spatial associations between the flood inventory and the explanatory variables was carried out using the EBF model, through which the flood susceptibility index (FSI) was derived. The FSI was classified using the geometrical interval classification scheme into five flood susceptibility classes. The model was validated using the relative operating characteristic (ROC) and area under the curve (AUC). The analysis demonstrated that the AUC values for the success and prediction rates were 0.778 and 0.816, respectively. These results validate the efficacy of the EBF model in accurately generating flood susceptibility maps for the study area.

Keywords: Evidential belief function, Dempster-Shafer, Flood susceptibility, Geographic Information System, Lam Chiang Krai

1. Introduction

Flooding is a natural disaster caused by climatic conditions and terrestrial surface characteristics. It has resulted in economic losses and adverse impacts on human life, as well as the destruction of physical assets, including farm machinery, agricultural land, crops, residential buildings, and critical infrastructure such as roads, bridges, and rail networks, while also causing damage to the surrounding natural environment [1]. The resulting damages often require substantial financial resources for recovery and rehabilitation. Flood disasters around the world exhibit diverse occurrence patterns and impacts, which are influenced by climatic factors, topographic conditions, and land use characteristics specific to each region. Southeast Asia is considered one of the regions most impacted by natural disasters, often driven by climatic factors and increasing in both frequency and intensity [2] and [3].

In the Southeast Asia region, Thailand is identified as one of the countries increasingly subjected to intense flooding events with rising occurrence rates. The substantial flooding was mostly caused by torrential rain and several tropical storms that occurred throughout the extended rainy season, with most events occurring during the later part of the monsoon period, spanning from August to November [4]. The predominant causes of flooding in Thailand are attributed to excessive rainfall [5], rapid urbanization, deforestation in the uplands, and insufficient flood management systems [6]. Flooding has led to significant economic losses in Thailand. According to the report [7], in late 2011, the most severe flood in seven decades inundated over one-third of the country, resulting in property and economic losses exceeding one trillion baht.

In 2011, the estimated indirect economic losses led to a 4.81% decrease in the country's gross domestic product (GDP), excluding transboundary impacts. Furthermore, these losses are projected to cause a GDP reduction exceeding 0.5% by 2030, culminating in total damages amounting to $55.3 billion between 2011 and 2030 [8]. Given these challenges, flood susceptibility mapping constitutes a critical preliminary step for the flood early warning system, the provision of emergency response services, future flood mitigation and prevention efforts, and the implementation of effective flood management plans [9][10] and [11]. This study focuses on selecting watersheds that have experienced flooding events, specifically characterizing them as small agricultural watersheds, to develop a model applicable to other agricultural areas facing similar challenges. The Lam Chiang Krai agricultural watershed, located near the edge of the Khorat Plateau in Nakhon Ratchasima province, is one such area that frequently experiences flooding issues. The selection of the Lam Chiang Krai watershed as the study area is based on several important considerations that enhance its relevance for flood susceptibility mapping. First, the watershed is representative of small agricultural basins situated along the Khorat Plateau, sharing similar geomorphological and land-use characteristics with many other flood-prone areas in northeastern Thailand. Second, recurrent flooding has been observed in the Lam Chiang Krai watershed over the past several decades, significantly impacting local agricultural productivity and livelihoods, thereby making it a critical area for the development of flood management measures. Furthermore, it is located in a socio-economically important region where agriculture serves as the main source of income for rural communities. Therefore, the results of this study can be used as a guideline for other agricultural watersheds in the region that experience similar hydrological, environmental, and socio-economic conditions.

Various modeling techniques have been employed globally by researchers to assess flood susceptibility. These methods include Multi-Criteria Decision Analysis (MCDA) [12], Analytical Hierarchy Process (AHP) [13], Frequency Ratio (FR) [14], Fuzzy-AHP [15], Logistic Regression (LR) [16] and [17], Fuzzy Logic [18], Support Vector Machine (SVM) [19], ensemble weights-of-evidence and SVM [20], Fuzzy Gramma Operator [21], integration of nature-inspired algorithms into support vector regression (SVR) [22], Metaheuristic Optimization Algorithms [23] and [24], Machine Learning, MCDA, and Ensemble using Dempster Shafer Theory [25]. These various models have been integrated with Geographic Information Systems (GIS) for assessing flood susceptibility. Traditional approaches such as the MCDA, AHP, and FR are widely applied due to their simplicity and interpretability [26]. However, these methods often rely on assumptions of linearity and expert judgment, which may introduce subjectivity and reduce their adaptability to complex or uncertain environments. In contrast, machine learning models such as SVM and metaheuristic algorithms offer high predictive performance but generally function as "black-box" models, limiting transparency and interpretability in spatial decision-making [20] and [27]. The Dempster-Shafer theory, meanwhile, provides a flexible probabilistic framework that effectively manages uncertainty and integrates multiple sources of evidence. It allows for spatial modeling of belief, disbelief, plausibility, and uncertainty, making it appropriate for flood susceptibility assessment in data-limited or heterogeneous environments [28].

The evidential belief function (EBF), grounded in the Dempster-Shafer theory of evidence, provides a mathematical foundation for reasoning in the presence of uncertainty and has been widely recognized as a robust approach for integrating spatial datasets [29]. The theory is particularly useful in situations where evidence is incomplete, imprecise, or uncertain, and it allows for the combination of evidence from different sources [30]. The knowledge-driven approach of the evidential belief function model has been used in flood susceptibility mapping [19][31] and [32]. The integration of GIS with the EBF model presents a powerful approach to natural disaster susceptibility mapping [19] and [29]. The main objective of this paper is to examine the potential application of the GIS and EBF model to flood susceptibility mapping in the Lam Chiang Krai watershed, Nakhon Ratchasima province, Northeast Thailand.

2. Materials and Methods

Figure 1 illustrates the methodological framework employed in this study. The dependent variable comprised historical flood records, subsequently partitioned into separate subsets for model development and accuracy assessment. This study employs frequently used factors in flood susceptibility mapping, including the elevation, slope, curvature, SPI, TWI, distance to stream, geology, soil texture, LULC, and mean annual rainfall [33]. An evaluation of multicollinearity was performed to identify potential redundancy within the set of independent variables [32]. The flood susceptibility index (FSI) was analyzed using the EBF model within a GIS environment.

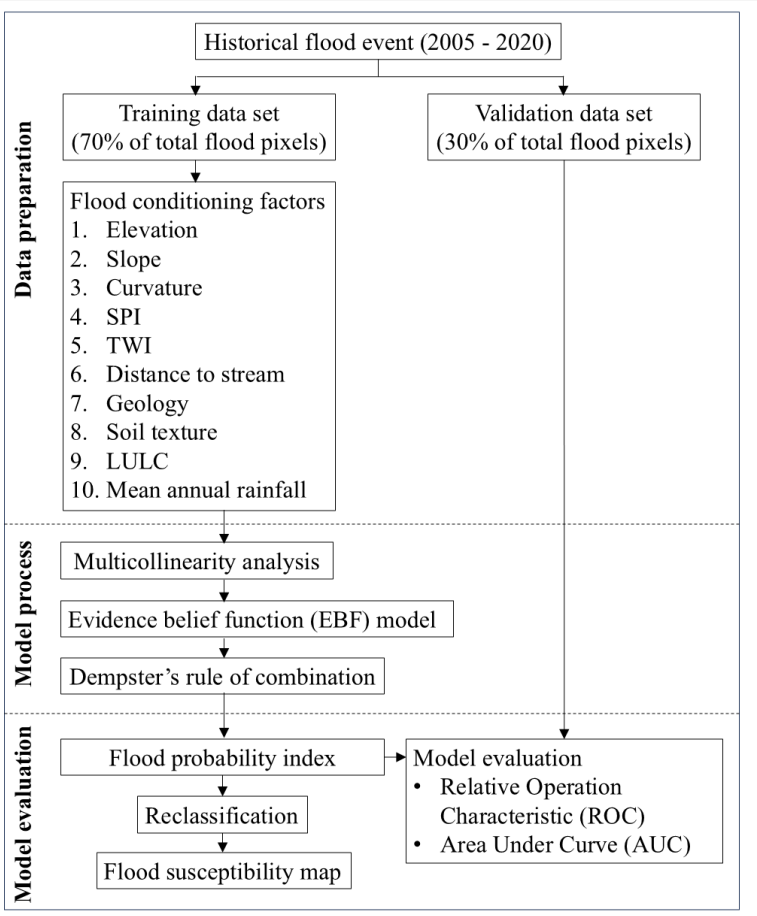

Figure 1: Flood susceptibility mapping methodology

The accuracy of the model was evaluated through the application of the relative operating characteristic (ROC) curve and the area under the curve (AUC) approach [34]. Subsequently, the FSI was reclassified to produce flood susceptibility maps.

2.1 Study Area

The Lam Chiang Krai watershed was selected as the study area, characterized by its predominantly agricultural landscape and previous significant flood damage. The watershed is suited to the edge of the Khorat Plateau, encompassing an area of 2,841 km^2. It is geographically located between 101° 25′ 39″ E to 102° 17′ 16″ E longitude and 14° 58′ 58″ N to 15° 17′ 56″ N latitude, in Nakhon Ratchasima province, Northeast, Thailand (Figure 2). The elevation ranges from 162 to 595 m.s.a.l., with an average elevation of approximately 226 m.s.a.l. The climate of the region is classified as a tropical savanna climate, with an annual mean temperature of 27.3°C. An average annual precipitation of 1,112 mm is received in the area, with the lowest mean monthly rainfall recorded in December (2.7 mm) and the highest in September (228.3 mm). The study area is geologically situated within Cretaceous sedimentary rock formations, primarily composed of sandstone and siltstone, including the Phu Phan, Khok Kruat, and Maha Sarakham Formations. Additionally, the downstream area of the watershed consists of Quaternary alluvial deposits. Land use in the area is primarily composed of agricultural activities, accounting for 86% of the total land, with 48% allocated to field crops and 35% to paddy fields.

2.2 Flood Inventory

The database of historical flood events is considered an important resource for examining the relationship between flood conditioning factors and flood occurrences [35] and [36]. The accuracy of historical flood event data is considered essential to the reliability of model outputs, as such data are utilized to train the model. In this study, the flood inventory was prepared using records of flood events from 2005 to 2020, which were interpreted using satellite imagery and provided by the Geo-Informatics and Space Technology Development Agency (GISTDA). The flood polygon data was provided in shapefile format and subsequently converted to raster format

with a 30 m spatial resolution. The coding for flooded and non-flooded areas was assigned as 1 and 0, respectively. The first step in developing an effective model is selecting datasets for training and validation. In other studies, flood raster data is often randomly sampled to create points for modeling. However, because flood events typically cover large areas (areal phenomena), representing them as points can introduce significant errors and distort the depiction of flood hazard zones [37]. To mitigate the aforementioned issue, this study recommends a more accurate method by using areal flood pixels rather than random sampling from flood areas. The flood inventory map contained 817,404 pixels representing flood conditions, which were split into two groups, with 609,283 pixels (70%) allocated for model training and 261,121 pixels (30%) for validation (Figure 2). The 70:30 ratio has been widely adopted in spatial modeling and machine learning studies, as it ensures an adequate sample size for model calibration while retaining a sufficient portion of data for independent validation, thereby enabling a reliable assessment of model performance [31] and [32].

2.3 Flood Conditioning Factors

Specific guidelines have not been defined for identifying flood conditioning factors influencing flood occurrences [38]. The selection of flood conditioning factors was based on the physical characteristics of the watershed, related research documents [33], and the availability of spatial data. These factors were derived from raw data obtained from several official agencies, with details presented in Table 1. Each factor was transformed into a raster data structure with a spatial resolution of 30 meters to enable consistent spatial analysis. All raster layers were subsequently converted to a 32-bit floating-point format to enable the representation of decimal values.

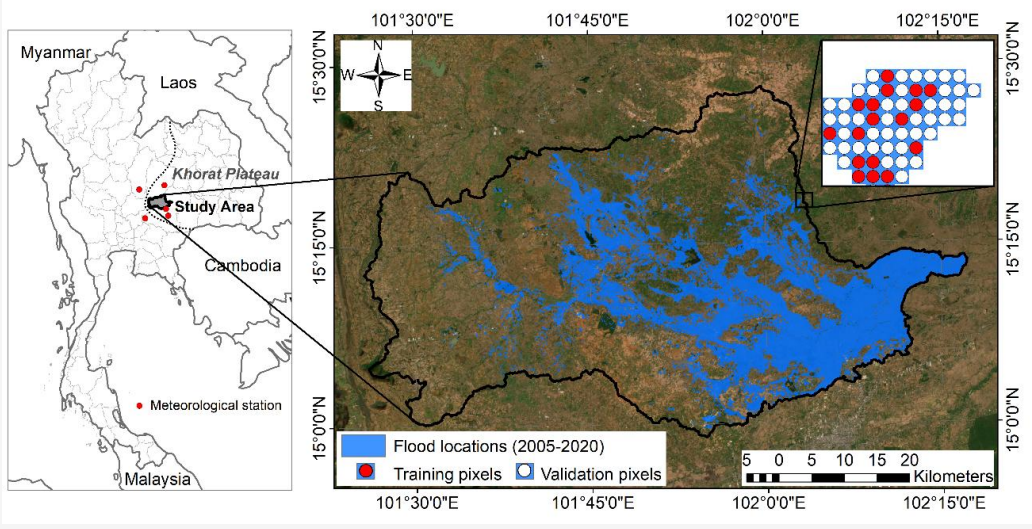

Figure 2: Flood data, and the division of datasets for model training and validation in Lam Chiang Krai Watershed, Nakhon Ratchasima Province, Thailand

Table 1: Spatial database used in the study

Source	GIS data	Data type	Description
GISTDA (https://disaster.gistda.or.th/flood/)	Flood inventory	Vector data	Flood events occurring between 2005 and 2020 were derived from various sources of satellite imagery.
Royal Thai Survey Department (RTSD) (https://www.rtsd.mi.th/)	Elevation, Slope, Curvature, SPI, TWI	Raster data	DEM spatial resolution 30 m, 15′ × 15′ tiles.
	Distance to stream	Vector data	Topographic map at a scale of 1:50,000.
Department of Mineral Resources (DMR) (https://www.dmr.go.th/)	Geology	Vector data	Geological map at a scale of 1:50,000.
Land Development Department (LDD) (https://www.ldd.go.th/)	Soil texture	Vector data	Soil map at a scale of 1:50,000.
	LULC	Vector data	LULC map at scale of 1:25,000.
Thai Meteorological Department (https://www.tmd.go.th/)	Mean annual rainfall	Point data	Meteorological station and climate data (1994 - 2023)

2.3.1 Elevation

It is well established that elevation is ranked among the most important factors influencing flood occurrence. Generally, a higher likelihood of flooding is associated with low-elevation areas, while a lower probability is linked to higher elevations [39]. Digital Elevation Models (DEM) are commonly used as the source for obtaining elevation data [33]. Therefore, the accuracy of the DEM parameters is considered essential to ensuring the validity of the flood susceptibility map [40]. Elevation values within the study area, ranging from 162 to 595 m.a.s.l., were classified into ten classes using the natural breaks method (Figure 3(a)).

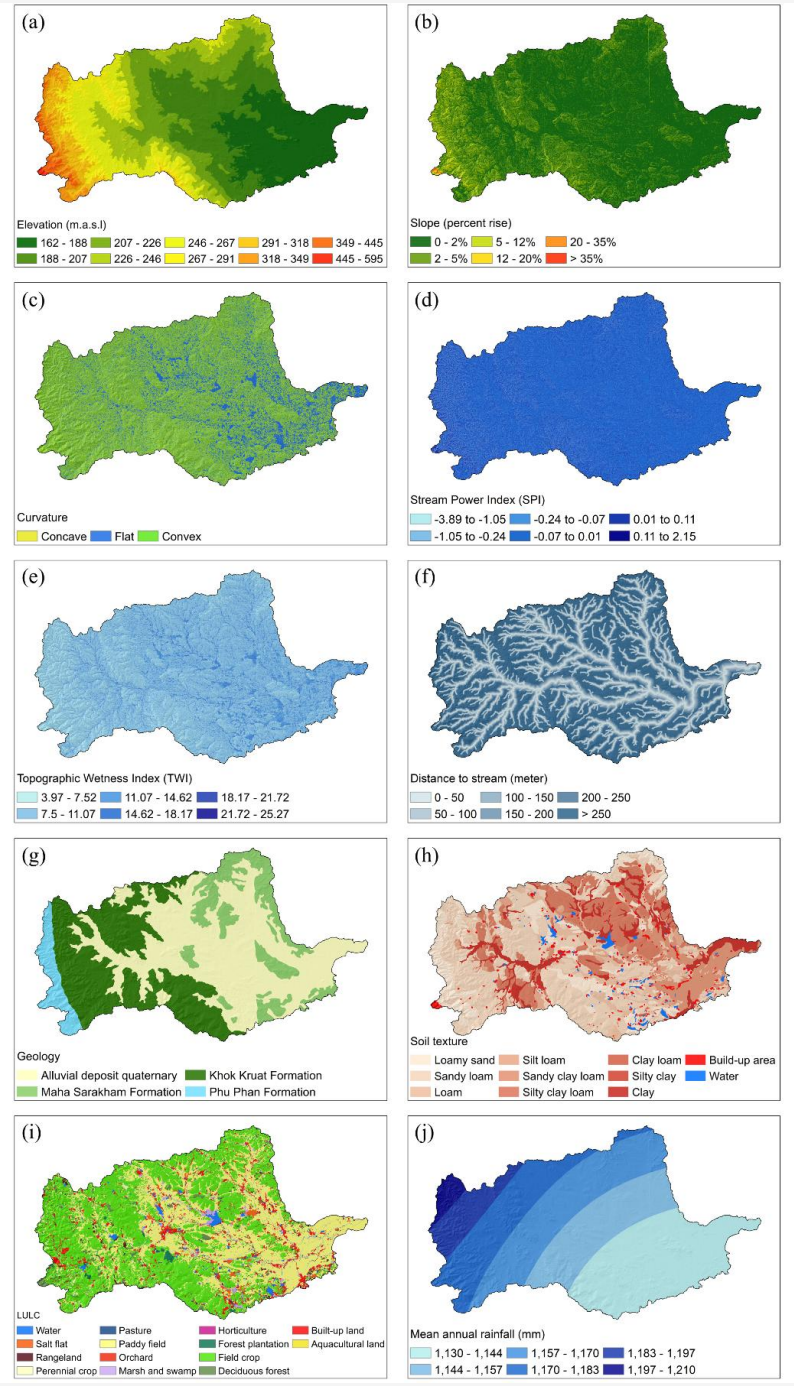

Figure 3: Flood conditioning factors; (a) elevation, (b) slope, (c) curvature, (d) SPI, (e) TWI, (f) distance to stream, (g) geology, (h) soil texture, (i) LULC, and (j) mean annual rainfall

2.3.2 Slope

The gradient of the terrain plays a significant role in influencing flood occurrence by affecting the gravitational force acting on the velocity of surface runoff. Steep slopes generally enable more rapid drainage, whereas flatter areas typically exhibit reduced flow efficiency, thereby increasing the likelihood of prolonged surface water accumulation and inundation [27] and [41]. The slope percent map was generated from the DEM layer using the Surface tool in ArcGIS. The slope of the study area ranges from 0 to 68.33%, with a mean of 1.75%, indicating predominantly gentle topographic features. The slope was classified into six classes: 0-2% (flat to nearly flat), 2-5% (gently undulating), 5-12% (undulating), 12-20% (rolling), 20-35% (hilly), and greater than 35% (steep) (Figure 3(b)).

2.3.3 Curvature

Curvature influences water flow dynamics and plays a significant role in flood occurrence [42]. It was derived from a DEM using the Curvature tool in ArcGIS [43] and reclassified into three categories: concave (negative values), convex (positive values), and flat (zero) (Figure 3(c)). The study area comprises 30%, 23%, and 47% of concave, convex, and flat areas, respectively.

2.3.4 Stream Power Index (SPI)

The SPI, which is influenced by slope and catchment area, is associated with water flow and sediment transport and is frequently utilized as a parameter in flood susceptibility assessments [41] and [44]. The flow energy and sediment mobilization capacity within a channel are evaluated using the SPI, which is calculated from the upslope contributing area and surface gradient [42], as shown in Equation [45].

$$SPI = A_s \cdot \tan\beta$$

Equation 1

Where A_s denotes the contributing drainage area (m^2m^{-1}), and tanβ represents the gradient expressed in degrees at that point [25]. The SPI was calculated using DEM data as input through the Raster Calculator tool in ArcGIS and was subsequently classified into six classes using the natural breaks method (Figure 3(d)).

2.3.5 Topographic wetness index (TWI)

The TWI is critical for analyzing hydrological processes and evaluating the influence of topographic features on surface runoff and water accumulation within a watershed [46]. Regions characterized by elevated TWI are typically more susceptible to flood inundation, as they signify areas of greater wetness [46]. The TWI is computed using Equation 2:

$$TWI = \ln\left(\frac{A_s}{\tan\beta}\right)$$

Equation 2

Where A_s and tanβ are as previously defined. The calculation was performed using the Raster Calculator tool in ArcGIS. The TWI was then classified into six classes using the equal interval method (Figure 3(e)).

2.3.6 Distance to stream

It is inherently evident that flood occurrence is influenced significantly by proximity to watercourses, as flood levels are typically extended outward from the river channel. Streams with higher stream orders have larger drainage areas, resulting in a greater influence on the extent of flood-prone areas compared to lower-order streams. Flood occurrences are predominantly observed in areas located in close proximity to 4th-, 5th-, and 6th-order streams within the watershed. The classification of stream hierarchy was conducted based on Strahler's stream ordering technique [47]. Adaptive buffering was applied based on the stream order, allowing buffer zones to vary in size according to the stream order (Figure 3(f)).

2.3.7 Geology

The geological characteristics of a watershed play a significant role in the analysis of flood-prone areas, as each lithological unit possesses distinct hydrological properties that influence water permeability and distribution [25]. Regions characterized by highly permeable soils and resistant rock formations tend to have lower stream density, influencing flood dynamics significantly [48]. According to the geological map provided by the DMR, the geological structure of the Lam Chiang Krai watershed predominantly consists of sedimentary rocks from the Cretaceous period, primarily sandstone and siltstone, which belong to the Phu Phan, Khok Kruat, and Maha Sarakham Formations. These formations influence permeability and water retention, which affect stream density and flood dynamics. The downstream area is predominantly characterized by Quaternary alluvial deposits, which may enhance water accumulation and increase flood potential due to their lower permeability and flat topography (Figure 3(g)).

2.3.8 Soil texture

Surface runoff, infiltration, and percolation rates within an area are greatly influenced by the characteristics of soil texture, which play a crucial

role in flood behavior [49]. Fine-textured soils are more susceptible to flooding and are generally less effective for groundwater recharge due to their reduced water infiltration rates. In contrast, coarse-textured soils, characterized by larger pore spaces, allow for greater infiltration, thereby decreasing flood susceptibility compared to finer-grained soils. This variation in soil texture results in differing capacities for water absorption across soil types [50]. According to the soil series map provided by the LDD, the Lam Chiang Krai watershed exhibits the following soil texture distribution: loamy sand (13%), sandy loam (36.4%), sandy clay loam (8.9%), loam (9.1%), silt loam (2%), clay loam (0.1%), silty clay loam (17.2%), silty clay (0.1%), and clay (8.4%). Additionally, two categories, water bodies (1.5%) and built-up areas (3.3%), which were excluded from the soil texture classification, were identified as low infiltration capacity areas (Figure 3(h)).

2.3.9 Land Use and Land Cover (LULC)

Surface runoff, sediment transport, and flood potential within a watershed are markedly affected by LULC characteristics [51]. Flood susceptibility tends to decrease in areas covered by dense forest or healthy vegetation, as the high density enhances infiltration rates, thereby reducing the likelihood of flooding [52]. Conversely, urban and built-up areas with impervious surfaces are more vulnerable to flooding, as these surfaces limit water infiltration and contribute to increased surface runoff accumulation. The dominant LULC types in the study area are field crops (48.34%), paddy fields (35.41%), and built-up land (5.66%), with other land use categories comprising smaller proportions (Figure 3(i)).

2.3.10 Mean annual rainfall

Rainfall serves as a primary hydrometeorological variable that substantially contributes to the initiation and severity of flood events [46]. According to data from the TMD, the Lam Chiang Krai watershed recorded a minimum annual rainfall of 573.90 mm in 2019 and a maximum of 1,852.40 mm in 2008. The highest monthly rainfall typically occurs in September, a period during the late rainy season when soil saturation has often reached its peak, thereby increasing the likelihood of flooding. The mean annual rainfall for this study was calculated using rainfall records from 1994 to 2023, obtained from five stations surrounding the study area (Figure 1). Spatial interpolation of rainfall data was carried out using the Inverse Distance Weighted (IDW) method to produce a rainfall distribution map [36], which was subsequently classified into six classes using the equal interval method (Figure 3(j)).

2.4 Multicollinearity Analysis

A key factor in selecting independent variables for analysis is evaluating the extent to which the variables are independent from one another. In cases where pairs of factors exhibit high correlations, multicollinearity may occur, potentially leading to analytical bias or distortion in the model's estimations. Two commonly used indices for diagnosing multicollinearity are tolerance (TOL) and the variance inflation factor (VIF) [53]. Tolerance is defined as the 1-R^2 value obtained from a regression in which the independent variable of interest is regressed on all other independent variables, excluding the dependent variable. Conversely, the VIF is calculated as the inverse of the TOL value [53]. According to established statistical guidelines, a variable is considered to be affected by multicollinearity if its TOL value is less than 0.1 and its VIF is equal to or greater than 5 [32]. Conversely, thresholds of VIF less than 5 and TOL greater than 0.1 are generally accepted as reflecting an acceptable level of multicollinearity, suggesting that the predictor variables exhibit sufficient independence for reliable regression analysis [54] and [55]. The VIF and TOL are calculated using Equations 3 and 4 [55]:

$$VIF_i = \frac{1}{1 - R_i^2}$$

Equation 3

$$TOL_i = \frac{1}{VIF_i}$$

Equation 4

VIF_i is the variance inflation factor value for the variable x_i, and R_i^2 is the coefficient of determination between x_i and all other variables. TOL_i is the tolerance value for the variable x_i. A high VIF value for a given variable is interpreted as an indication of strong linear association with other independent variables [55]. The VIF was derived through the application of the Exploratory Regression tool available in the Spatial Statistics toolbox of ArcGIS software.

2.5 Evidential Belief Function (EBF) Model

The Dempster-Shafer theory of evidence is also referred to as the EBF [56]. This model is primarily based on the theoretical framework established by [57] and further developed by [30] and [58]. The EBF model is grounded in an evidence-based approach, in which observed evidence is utilized to estimate probabilities through belief functions. Within this framework, uncertainty, disbelief, and plausibility are also assessed, and these components are integrated to evaluate the likelihood of event

occurrence [59]. The application of the EBF model within a GIS environment involves the use of *n* spatial data layers associated with flood-related factors. Each of these layers is considered to correspond to a specific piece of evidence, denoted as E_i (E_1, E_2, …, E_n), which contributes to the evaluation of flood susceptibility. Each spatial data layer is composed of *j*th attribute classes, represented by the symbol E_{ij}, which serve as evidence contributing to the flood susceptibility assessment [29]. The positive and negative likelihood ratios are derived from the evidential information based on the observed evidence [30]. The likelihood ratio $\lambda(T_P)_{Eij}$ is computed to express the degree of support provided by the evidence E_{ij} for the presence of flooding, as shown in Equation 5 [29]:

$$\lambda(T_P)_{E_{ij}} = \frac{\frac{N(F \cap E_{ij})}{N(F)}}{\frac{N(E_{ij}) - N(F \cap E_{ij})}{N(A) - N(F)}}$$

Equation 5

Where $N(F \cap E_{ij})$ represents the count of flood pixels that intersect with the class E_{ij}. $N(F)$ denotes the overall number of flood pixels within the study region, while $N(E_{ij})$ refers to the number of pixels in class E_{ij}. $N(A)$ indicates the total pixel count across the entire study area. The value in the numerator reflects the proportion of flood pixels associated with the specific attribute E_{ij}, whereas the denominator corresponds to the proportion of non-flood pixels within that same class [29]. The belief function (*Bel*) is calculated as (Equation 6):

$$Bel = \frac{\lambda(T_P)_{E_{ij}}}{\sum \lambda(T_P)_{E_{ij}}}$$

Equation 6

The likelihood ratio to quantify the degree to which the evidence E_{ij} supports the absence of flooding, as presented in Equation 7:

$$\lambda(\overline{T}_P)_{E_{ij}} = \frac{\frac{N(F) - N(F \cap E_{ij})}{N(F)}}{\frac{N(A) - N(F) - N(E_{ij}) + N(F \cap E_{ij})}{N(A) - N(F)}}$$

Equation 7

Where $\lambda(\overline{T}_P)_{E_{ij}}$ denotes the likelihood ratio supporting the hypothesis of flood absence over its occurrence. In the numerator, the proportion of flood-absent pixels corresponding to the specified attribute class E_{ij} is determined, while in the denominator, the proportion of non-flood pixels across the remaining attribute classes is evaluated [29]. The disbelief function (*Dis*) is calculated as (Equation 8):

$$Dis = \frac{\lambda(\overline{T}_P)_{E_{ij}}}{\sum \lambda(\overline{T}_P)_{E_{ij}}}$$

Equation 8

The uncertainty (*Unc*) and plausible (*Pls*) measures are computed based on Equation 9 and Equation 10:

$$Unc = 1 - Dis - Bel$$

Equation 9

$$Pls = 1 - Dis$$

Equation 10

In a GIS environment, the computation of *Bel*, *Dis*, *Unc*, and *Pls* values across all classified units within each raster layer can be performed by overlaying maps using the combine function. The number of flood and non-flood pixels within each class is counted during this step, and the resulting values can be exported for further calculations in Excel (Figure 4). The calculated *Bel*, *Dis*, *Unc*, and *Pls* values are then assigned to each class of each factor. Dempster's Rule of Combination (DRC) has been employed to overlay spatial layers for the purpose of generating four integrated EBF maps [19]. Assuming that two flood-related data layers, referred to as *A* and *B*, are considered, the integration is carried out using the following equations [60]:

$$Bel_x = \frac{Bel_A Bel_B + Bel_A Unc_B + Bel_B Unc_A}{1 - Bel_A Dis_B - Dis_A Bel_B}$$

Equation 11

$$Dis_x = \frac{Dis_A Dis_B + Dis_A Unc_B + Dis_B Unc_A}{1 - Bel_A Dis_B - Dis_A Bel_B}$$

Equation 12

$$Unc_x = \frac{Unc_A Unc_B}{1 - Bel_A Dis_B - Dis_A Bel_B}$$

Equation 13

EBF maps of each factor are combined pairwise using DRC, and the resulting output from the initial combination is subsequently integrated with the next factor. The output layer is subsequently combined with another factor, and this process continues until only a single pair of factors remains [32].

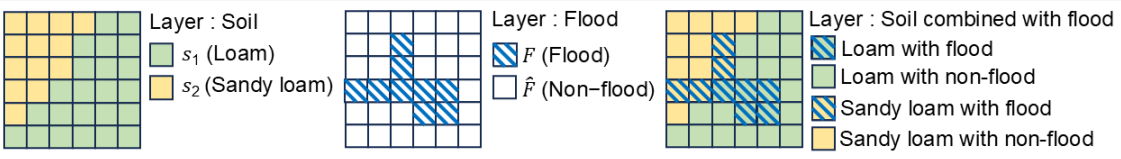

EBF

Layer : Soil	Class pixels	Flood pixels	$\lambda(T_p)$	$\lambda(\overline{T_p})$	Belief	Disbelief	Uncertainty	Plausible
Loam (s_1)	23	5	0.024	1.333	0.413	0.615	-0.029	0.385
Sandy loam (s_2)	13	4	0.035	0.833	0.587	0.385	0.029	0.615
Total	36	9	0.059	2.167	1.000	1.000	0.000	1.000

Figure 4: Example of applying the EBF model to calculate values for raster grid cells

Table 2: Multicollinearity analysis for flood conditioning factors

Flood conditioning factor	VIF	Tolerance
Elevation	4.29	0.23
Slope	2.92	0.34
Curvature	1.72	0.58
SPI	3.16	0.32
TWI	1.76	0.57
Distance to stream	1.22	0.82
Geology	1.89	0.53
Soil texture	1.09	0.92
LULC	1.02	0.98
Mean annual rainfall	2.78	0.36

2.6 Validation

Model accuracy assessment is a necessary step for indicating both the effectiveness and reliability of the model within the analytical framework [61]. The ROC method is widely employed for model validation, as it offers a quantitative approach to compare binary reference data with index-based prediction outputs. An AUC value of 1.0 signifies a perfect match between the predicted high flood probability and the actual flood occurrence. In contrast, a randomly generated flood probability map results in a diagonal ROC curve, yielding an AUC of 0.5 [34]. Therefore, AUC scores approaching 1.0 reflect strong predictive performance, whereas a ROC curve falling below the diagonal line indicates poor predictive accuracy regarding flood occurrence [1]. In the present study, flood data employed for model accuracy evaluation were split into two subsets: 70% of the dataset was allocated for analyzing the model's success rate, while the remaining 30% was reserved for prediction rate assessment. The ArcSDM, a Python-based ArcGIS toolbox [62], was utilized in this study to calculate the AUC.

3. Results and Discussions

3.1 Multicollinearity Analysis

Multicollinearity among the flood conditioning variables was assessed through the VIF and TOL. As presented in Table 2, all VIF values remain under the threshold of 5, and TOL values are above 0.1, suggesting an absence of serious multicollinearity issues. Therefore, all selected conditioning factors were retained for subsequent flood susceptibility modeling.

3.2 Flood Susceptibility Mapping by EBF model

The likelihood ratio supports the belief that floods (Equation 5) and the opposite target proposition (Equation 7) were first computed, and then belief (Equation 6), disbelief (Equation 8), uncertainty (Equation 9), and plausible function (Equation10) were finally derived. Table 3 shows the result of the EBF model in the case of each flood conditioning factor. This study examined flood susceptibility using the Bel and Pls indicators, derived from the EBF. For elevation, areas ranging from 162 to 188 meters exhibited the highest flood susceptibility, with Bel and Pls values of 0.533 and 0.951, respectively. In contrast, susceptibility decreased in higher elevation classes, confirming a negative correlation between elevation and flood likelihood. The low-lying eastern region of the Lam Chiang Krai watershed was identified as particularly vulnerable to flood hazards. Flat areas with slopes ranging from 0 to 2% exhibited the highest flood susceptibility, with Bel and Pls values of 0.751 and 0.950, respectively.

Table 3: Calculated *Bel*, *Dis*, *Unc*, and *Pls* values for each class within the thematic layers (Cont. next page)

Factor	Class	Class pixels	Flood pixels	EBF			
				Bel	***Dis***	***Unc***	***Pls***
Elevation (m)	162-188	669,315	347,344	0.533	0.049	0.418	0.951
	188-207	669,768	173,660	0.266	0.089	0.645	0.911
	207-226	519,889	55,735	0.110	0.111	0.779	0.889
	226-246	407,304	19,380	0.049	0.114	0.837	0.886
	246-267	373,563	11,192	0.031	0.115	0.855	0.885
	267-291	197,481	1,697	0.009	0.108	0.883	0.892
	291-318	165,016	275	0.002	0.107	0.891	0.893
	318-349	103,444	0	0.000	0.104	0.896	0.896
	349-445	47,584	0	0.000	0.102	0.898	0.898
	445-595	3,927	0	0.000	0.100	0.900	0.900
Slope (%)	0-2 (flat to nearly flat)	2,171,271	547,384	0.751	0.050	0.199	0.950
	2-5 (gently undulating	870,107	60,372	0.207	0.234	0.559	0.766
	5-12 (undulating)	111,688	1,526	0.041	0.185	0.775	0.815
	12 – 20 (rolling)	2,142	1	0.001	0.177	0.821	0.823
	20 – 35 (hilly)	1,523	0	0.000	0.177	0.823	0.823
	> 35 (steep)	560	0	0.000	0.177	0.823	0.823
Curvature	Concave (-)	1,127,328	183,784	0.281	0.367	0.352	0.633
	Convex (+)	994,865	142,051	0.246	0.382	0.372	0.618
	Flat (0)	1,035,098	283,448	0.472	0.251	0.276	0.749
SPI	-3.89 to -1.05	703	0	0.000	0.169	0.831	0.831
	-1.05 to -0.24	156,789	5,233	0.048	0.178	0.774	0.822
	-0.24 to -0.07	709,536	108,472	0.220	0.181	0.599	0.819
	-0.07 to 0.01	1,317,372	354,189	0.387	0.114	0.500	0.886
	0.01 to 0.11	863,741	131,878	0.220	0.185	0.595	0.815
	0.11 to 2.15	109,150	9,511	0.125	0.173	0.702	0.827
TWI	3.97 to 7.52	745,914	71,874	0.052	0.198	0.750	0.802
	7.52 to 11.07	1,711,472	313,037	0.099	0.178	0.723	0.822
	11.07 to 14.62	588,693	187,415	0.172	0.135	0.692	0.865
	14.62 to 18.17	89,278	27,911	0.169	0.161	0.670	0.839
	18.17 to 21.72	17,789	6,732	0.205	0.164	0.631	0.836
	21.72 to 25.27	4,145	2,314	0.302	0.164	0.533	0.836
Distance to stream (m)	0 to 50	477,338	158,273	0.243	0.137	0.621	0.863
	50 to 100	421,407	122,490	0.213	0.146	0.641	0.854
	100 to 150	365,472	93,240	0.187	0.153	0.660	0.847
	150 to 200	316,900	68,836	0.159	0.159	0.682	0.841
	200 to 250	282,068	51,178	0.133	0.163	0.705	0.837
	> 250	1,294,106	115,266	0.065	0.243	0.691	0.757

Table 3: Calculated *Bel*, *Dis*, *Unc*, and *Pls* values for each class within the thematic layers (Cont. from previous page)

Factor	Class	Class pixels	Flood pixels	EBF			
				Bel	***Dis***	***Unc***	***Pls***
Geology	Alluvial deposit quaternary	1,537,847	538,070	0.739	0.049	0.212	0.951
	Maha Sarakham Formation	459,461	44,540	0.205	0.283	0.512	0.717
	Khok Kruat Formation	998,192	26,673	0.056	0.395	0.549	0.605
	Phu Phan Formation	161,791	0	0.000	0.273	0.727	0.727
Soil texture	loamy sand	411,872	28,686	0.024	0.101	0.875	0.899
	sandy loam	1,148,295	125,427	0.038	0.119	0.843	0.881
	loam	287,221	110,964	0.133	0.079	0.788	0.921
	silt loam	63,029	5,476	0.030	0.091	0.879	0.909
	sandy clay loam	281,816	177,681	0.218	0.066	0.716	0.934
	silty clay loam	542,175	38,035	0.024	0.105	0.871	0.895
	clay loam	3,219	1,662	0.178	0.089	0.732	0.911
	silty clay	2,394	285	0.041	0.090	0.869	0.910
	clay	266,472	78,477	0.102	0.084	0.814	0.916
	built - up area	103,123	24,913	0.083	0.089	0.828	0.911
	water	47,674	17,677	0.128	0.088	0.784	0.912
LULC	paddy field	1,117,864	447,878	0.120	0.025	0.855	0.975
	field crop	1,526,160	50,433	0.010	0.150	0.840	0.850
	perennial crop	41,091	1,987	0.015	0.070	0.916	0.930
	orchard	11,164	1,266	0.034	0.069	0.897	0.931
	horticulture	1,871	618	0.099	0.069	0.832	0.931
	pasture	12,311	2,141	0.052	0.069	0.879	0.931
	aquacultural land	5,571	2,404	0.130	0.069	0.802	0.931
	deciduous forest	41,582	1,589	0.011	0.070	0.919	0.930
	forest plantation	13,499	563	0.013	0.069	0.918	0.931
	rangeland	60,681	10,587	0.052	0.069	0.879	0.931
	marsh and swamp	39,237	20,410	0.156	0.067	0.777	0.933
	built-up land	178,859	31,851	0.053	0.069	0.877	0.931
	water body	78,992	21,124	0.080	0.068	0.852	0.932
	salt flat	28,409	16,432	0.174	0.067	0.759	0.933
Mean Annual Rainfall (mm)	1,130.96 to 1,144.18	962,383	371,660	0.497	0.085	0.418	0.915
	1,144.18 to 1,157.40	582,555	114,696	0.254	0.166	0.580	0.834
	1,157.40 to 1,170.61	757,576	90,153	0.153	0.193	0.654	0.807
	1,170.61 to 1,183.83	562,502	27,196	0.062	0.202	0.735	0.798
	1,183.83 to 1,197.05	223,149	5,492	0.032	0.181	0.787	0.819
	1,197.05 to 1,210.27	69,126	86	0.002	0.172	0.826	0.828

In contrast, steeper slopes showed a significantly lower likelihood of flooding due to increased runoff. For slopes greater than 12%, susceptibility was negligible, with Bel values reaching 0 in hilly and steep terrains where no flooding events were recorded. These findings suggest that gentle slopes are highly vulnerable to flooding, whereas steep slopes are far less prone to flood occurrences. In terms of curvature, flat areas, with Bel and Pls values of 0.472 and 0.749, respectively, exhibited a stronger association with flood occurrence compared to concave and convex areas. Flat areas with poor drainage systems exhibit the highest susceptibility to flooding, while concave areas have a moderate level of susceptibility. In contrast, convex areas are less prone to flood hazards due to their well-developed drainage systems.

The study indicates that flood susceptibility decreases as elevation increases and slope becomes steeper, resulting in reduced vulnerability in elevated and inclined regions compared to low-lying areas. The significance of terrain curvature was highlighted, indicating greater flood susceptibility in flat areas than in concave or convex landscapes, supported by existing literature [32][61][63] and [64]. Our findings are consistent with those of previous studies, in which flat or concave terrains were identified as having the highest likelihood of flood occurrence. For SPI, areas with values between -0.07 and 0.01 displayed the highest flood susceptibility (Bel = 0.387, Pls = 0.886), while extreme negative and positive values showed minimal susceptibility. Analysis of TWI revealed that areas with values greater than 21.75 had the highest susceptibility (Bel = 0.302, Pls = 0.836), indicating the role of moisture accumulation in flooding. In the case of distance to streams, a clear trend was observed: areas within 50 meters of streams exhibited the highest flood susceptibility (Bel = 0.243, Pls = 0.863), which decreased with greater distances. Regarding geology, alluvial deposits of the Quaternary period were most flood-prone (Bel = 0.739, Pls = 0.951), while formations like Maha Sarakham, Khok Kruat, and Phu Phan were less susceptible. For soil texture, sandy clay loam had the highest susceptibility (Bel = 0.218, Pls = 0.934), followed by clay and loam textures, reflecting their water retention characteristics. The LULC analysis indicated that paddy fields were most vulnerable (Bel = 0.120, Pls = 0.975) due to their low elevation and water dependency, whereas built-up land, forested areas, and perennial crops exhibited lower susceptibility. Finally, for mean annual rainfall, areas with 1,130.96–1,144.18 mm rainfall were highly susceptible (Bel = 0.497, Pls = 0.915), highlighting the influence of rainfall distribution on flooding patterns. Based on the Bel and Pls values of each layer, it was shown that flood susceptibility was most strongly correlated with low elevation, gentle slopes, flat terrain, alluvial deposits, and paddy fields. These conditions contributed to a higher likelihood of flooding. All input layers were overlaid and integrated using Dempster's rule of combination to generate the EBF maps: Bel, Dis, Unc, and Pls, as illustrated in Figure 5.

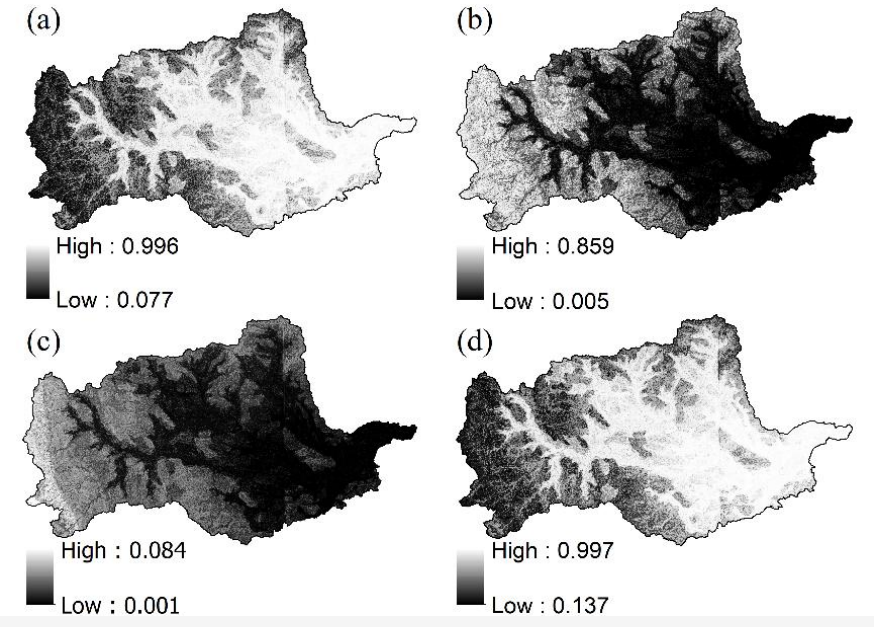

Figure 5: Integration results using the EBF model; (a) belief, (b) disbelief, (c) uncertainty, and (d) plausibility

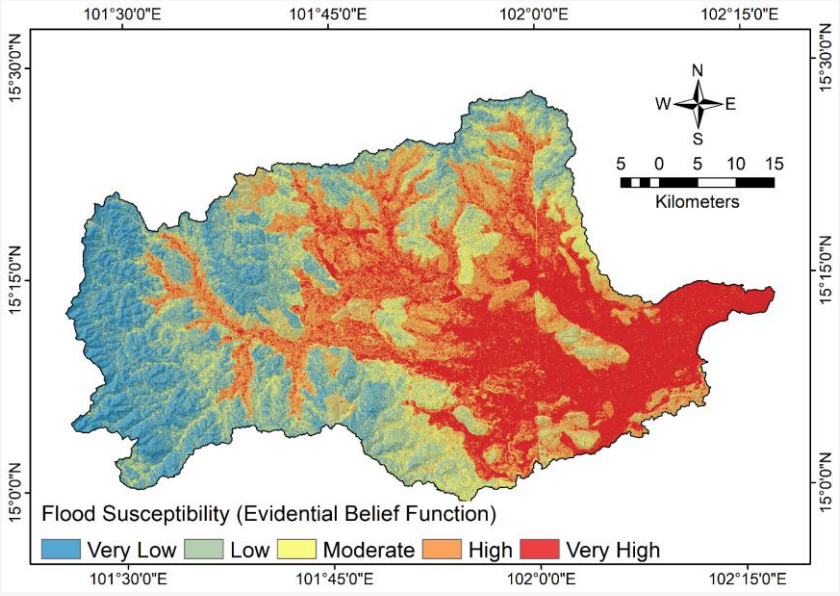

Figure 6: Flood susceptibility map

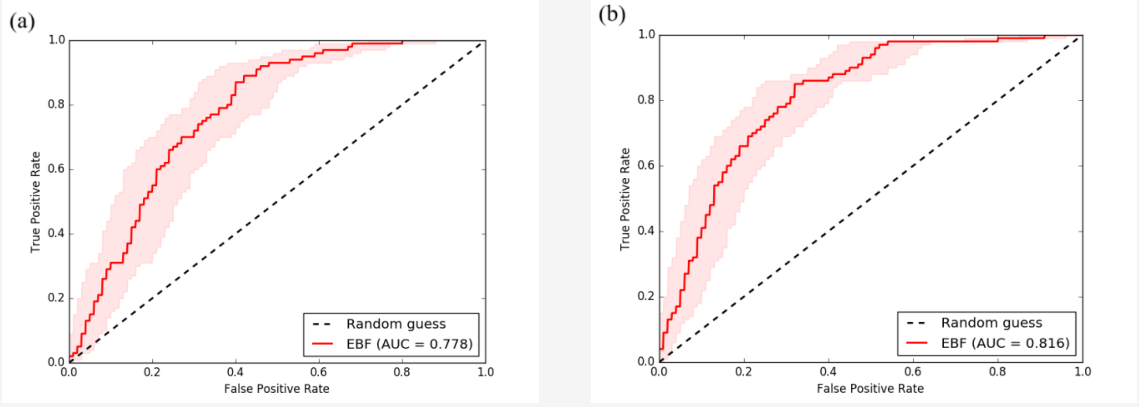

Figure 7: AUC values of the EBF model; (a) Success rate and (b) Prediction rate

The Bel function values ranged from 0.077 to 0.996, the Dis function values ranged from 0.005 to 0.859, the Unc function values ranged from 0.001 to 0.084, and the Pls function values ranged from 0.137 to 0.997. An inverse relationship was observed between the Bel and Dis functions, where areas with high Bel values corresponded to low Dis values. In this study, the Bel function was used to generate the FSI. The Bel values were classified into five susceptibility categories using the geometrical interval method (Figure 6) as follows: 0.077–0.265 (very low), 0.265–0.687 (low), 0.687–0.875 (moderate), 0.875–0.959 (high), and 0.959–0.996 (very high). The results of the EBF model indicated that a large portion (25.40%) of the study area was located in the very high susceptibility class, followed by the low (23.48%), high (20.42%), and moderate (16.33%) classes, with the smallest area (14.47%) classified as very low susceptibility.

3.3 Model Accuracy Evaluation

Validation of the flood susceptibility map was conducted using the ROC-AUC method, based on the training dataset for success rate and the validation dataset for prediction rate. The prediction rate was used as an indicator of the model's effectiveness and the explanatory power of the influencing factors in estimating flood occurrences. In this study, the AUC values of success and prediction rates were 0.778 (Figure 7(a)) and 0.816 (Figure 7(b)), respectively, indicating that the model was satisfied to create a flood susceptibility map in the study area. Several studies have reported similar findings about the reliability of using AUC values for flood susceptibility mapping.

For instance, [32] reported AUC values of 0.826 and 0.896 for the success and prediction rates, respectively, when using the evidential belief function for flood susceptibility assessment in Australia. Similarly, [28] achieved an AUC value of 0.879 for prediction rates in their study of flood susceptibility modeling in India using the evidential belief function and logistic regression model. The comparable results across different geographic locations and modeling techniques suggest the general applicability of the approach, enhancing its credibility.

4. Conclusion

Flood susceptibility mapping is a crucial strategy for flood preparedness. Reliable methods enhance the usability of flood susceptibility maps for mitigating flood damage. Building upon this concept, the results of an extensive investigation into flood vulnerability assessment within the Lam Chiang Krai watershed, Nakhon Ratchasima province, Thailand, have been reported. The first step of the study involved preparing a flood inventory map, as the effectiveness of model development depends on historical flood event data. This study proposes a more accurate approach by using areal flood pixels instead of randomly sampling from flood areas. Flood data were randomly divided into training and validation data. The inclusion of critical flood conditioning factors such as elevation, slope, curvature, SPI, TWI, distance to stream, geology, soil texture, LULC, and mean annual rainfall allowed for a detailed and accurate analysis of flood susceptibility. Multicollinearity analysis was conducted to ensure that the selected variables were not redundant. The combined belief function effectively quantified the flood susceptibility index, which was subsequently classified into five distinct susceptibility classes. The model's performance, validated using the ROC approach, produced AUC values of 0.778 for success rates and 0.816 for prediction rates. These results indicate that the EBF model is robust and satisfactory for mapping flood susceptibility in the study area. Overall, this study highlights the efficacy of using the EBF model in flood susceptibility modeling and offers a valuable tool for flood risk management and planning. The findings of this study can support planners in enhancing flood preparedness and mitigating the impacts of future flooding events. The map provides critical information to support land-use planning by identifying high-risk flood zones where development should be limited or carefully managed. It also informs flood mitigation strategies by prioritizing areas for structural measures such as drainage improvements and flood barriers, as well as non-structural approaches like community awareness and early warning systems. These applications aim to reduce flood damage, protect agricultural productivity, and enhance the resilience of local communities within the Lam Chiang Krai watershed. Finally, while the model performed well in this specific agricultural watershed, its transferability to areas with different hydrological or socio-environmental conditions requires further validation.

The EBF model demonstrates several key strengths in flood susceptibility mapping. Its ability to effectively integrate multiple sources of spatial evidence while explicitly managing uncertainty is a significant advantage, especially in complex and data-limited environments such as the Lam Chiang Krai watershed. The method's probabilistic framework allows for spatial representation of flood risk through belief, disbelief, uncertainty, and plausibility measures, providing more informative maps than other models. The EBF not only enables predictive mapping of flood susceptibility zones but also allows modeling of the degrees of uncertainty in the predictions. This capability is particularly valuable for decision-makers, as it provides a more comprehensive understanding of both the likelihood of flooding and the confidence level associated with each prediction. By quantifying uncertainty, the EBF model helps identify areas where further data collection or field verification is needed, ultimately improving the reliability and effectiveness of flood risk management strategies. When combined with GIS, the effectiveness of the EBF model is further enhanced, as GIS enables efficient spatial data processing, visualization, and management of large geospatial datasets. This integration supports the creation of high-resolution flood susceptibility maps that are essential for local-scale planning and decision-making. However, the approach is sensitive to the quality and completeness of input data; inaccuracies or biases in flood inventory or conditioning factors could propagate through the model and affect outcomes.

Future research should focus on integrating the EBF model with machine learning algorithms to combine the strengths of probabilistic reasoning and high predictive performance. A high-accuracy flood inventory should be developed in future studies. Additionally, incorporating temporal flood data and climate change projections could improve the model's relevance for long-term planning and dynamic flood risk assessment. Addressing the computational complexity of the EBF approach, particularly for large-scale applications, may be achieved through the development of automated data processing tools and optimized workflows.

Acknowledgement
This research was supported by the Research and Development Institute, Nakhon Ratchasima Rajabhat University. We express our gratitude to the reviewers who offered valuable suggestions on how to improve the manuscript's quality.

Reference

[1] Samanta, R. K., Bhunia, G. S., Shit, P. K. and Pourghasemi, H. R., (2018). Flood Susceptibility Mapping Using Geospatial Frequency Ratio Technique: A Case Study of Subarnarekha River Basin, India. *Model Earth Syst Environ*, Vol. 4(1), 395–408. https://doi.org/10.1007/s40808-018-0427-z.

[2] Ahern, M., Kovats, R. S., Wilkinson, P., Few, R. and Matthies, F., (2005). Global Health Impacts of Floods: Epidemiologic Evidence. *Epidemiol Rev*, Vol. 27(1), 36–46. https://doi.org/10.1093/epirev/mxi004.

[3] Torti, J. M. I., (2012). Floods in Southeast Asia: A Health Priority. *Journal of Global Health*, Vol. 2(2). https://doi.org/10.7189/jogh.02.020304.

[4] World Bank, (2012). *Thai flood 2011: Rapid Assessment for Resilient Recovery and Reconstruction planning: Overview*. Washington, D.C., Accessed: Aug. 02, 2024. [Online]. Available: http://documents.worldbank.org/curated/en/677841468335414861/Overview

[5] Gale, E. L. and Saunders, M. A., (2013). The 2011 Thailand flood: Climate Causes and Return Periods. *Weather*, Vol. 68(9), 233–237. https://doi.org/10.1002/wea.2133.

[6] Tanwattana, P., (2018). Systematizing Community-Based Disaster Risk Management (CBDRM): Case of Urban Flood-Prone Community in Thailand Upstream Area. *International Journal of Disaster Risk Reduction*, Vol. 28, 798–812. https://doi.org/10.1016/j.ijdrr.2018.02.010.

[7] Health Information System Development Office, (2022). Recurrence of Flood Disasters: Impact and Adaptations. Accessed: Aug. 02, 2024. [Online]. Available: https://www.hiso.or.th/hiso/picture/reportHealth/ThaiHealth2022/eng2022_23.pdf

[8] Tanoue, M., Taguchi, R., Nakata, S., Watanabe, S., Fujimori, S. and Hirabayashi, Y., (2020). Estimation of Direct and Indirect Economic Losses Caused by a Flood with Long-Lasting Inundation: Application to the 2011 Thailand Flood. *Water Resources Research*, Vol. 56(5). https://doi.org/10.1029/2019WR026092.

[9] Bubeck, P., Botzen, W. J. W. and Aerts, J. C. J. H., (2012). A Review of Risk Perceptions and Other Factors that Influence Flood Mitigation Behavior. *Risk Analysis*, Vol. 32(9), 1481–1495. https://doi.org/10.1111/j.1539-6924.2011.01783.x.

[10] Alshammari, E., Abdul Rahman, A., Ranis, R., Abu Seri, N., and Ahmad, F. (2024). Investigation of Runoff and Flooding in Urban Areas based on Hydrology Models: A Literature Review. *International Journal of Geoinformatics*, Vol. 20(1), 99–119. https://doi.org/10.52939/ijg.v20i1.3033.

[11] Tehrany, M. S., Shabani, F., Neamah Jebur, D. M., Hong, H, Chen, W. and Xie, X., (2017). GIS-based Spatial Prediction of Flood Prone Areas Using Standalone Frequency Ratio, Logistic Regression, Weight of Evidence and their Ensemble Techniques. *Geomatics, Natural Hazards and Risk*, Vol. 8(2), 1538–1561. https://doi.org/10.1080/19475705.2017.1362038.

[12] Edamo, M. L., Ukumo, T. T., Lohani, T. K., Ayana, M. T., Ayele, M. A., Mado, Z. M. and Abdi, D. M., (2022). A Comparative Assessment of Multi-Criteria Decision-Making Analysis and Machine Learning Methods for Flood Susceptibility Mapping and Socio-Economic Impacts on Flood Risk in Abela-Abaya Floodplain of Ethiopia. *Environmental Challenges*, Vol. 9. https://doi.org/10.1016/J.ENVC.2022.100629.

[13] Thammaboribal, P., Triapthti, N., and Lipiloet, S. (2025). Using of Analytical Hierarchy Process (AHP) in Disaster Management: A Review of Flooding and Landslide Susceptibility Mapping. *International Journal of Geoinformatics*, Vol. 21(4), 177–196. https://doi.org/10.52939/ijg.v21i4.4091.

[14] Duangyiwa, C. and Cheewinsiriwat, P., (2023). Flood Susceptibility Mapping Using a Frequency Ratio Model: A Case Study of Chai Nat Province, Thailand. In: Boonpook, W., Lin, Z., Meksangsouy, P., Wetchayont, P. (eds) Applied Geography and Geoinformatics for Sustainable Development. Springer Geography. Springer, Cham, 1–17. https://doi.org/10.1007/978-3-031-16217-6_1.

[15] Yaseen, Z. M., (2024). Flood Hazards and Susceptibility Detection for Ganga River, Bihar State, India: Employment of Remote Sensing and Statistical Approaches. *Results in Engineering*, Vol. 21. https://doi.org/10.1016/J.RINENG.2023.101665.

[16] Al-Juaidi, A. E. M., Nassar, A. M. and Al-Juaidi, O. E. M., (2018). Evaluation of Flood Susceptibility Mapping Using Logistic Regression and GIS Conditioning Factors. *Arabian Journal of Geosciences*, Vol. 11(24). https://doi.org/10.1007/s12517-018-4095-0.

[17] Waiyasusri, K., Wetchayont, P., Tananonchai, A. and Suwanmajo, D., (2023). Flood Susceptibility Mapping Using Logistic Regression Analysis in Lam Khan Chu Watershed, Chaiyaphum Province, Thailand. *Geography, Environment, Sustainability*, Vol. 16(2), 41–56.

[18] Gohil, M., Mehta, D. and Shaikh, M., (2024). An Integration of Geospatial and Fuzzy-Logic Techniques for Multi-Hazard Mapping. *Results in Engineering*, Vol. 21. https://doi.org/10.1016/J.RINENG.2024.101758.

[19] Tehrany, M. S., Kumar, L. and Shabani, F., (2019). A Novel GIS-based Ensemble Technique for Flood Susceptibility Mapping Using Evidential Belief Function and Support Vector Machine: Brisbane, Australia. *PeerJ*, Vol. 7. https://doi.org/10.7717/peerj.7653.

[20] Tehrany, M. S., Pradhan, B. and Jebur, M. N., (2014). Flood Susceptibility Mapping Using a Novel Ensemble Weights-Of-Evidence and Support Vector Machine Models in GIS. *Journal of Hydrology (Amst)*, Vol. 512, 332–343. https://doi.org/10.1016/j.jhydrol.2014.03.008.

[21] Ramesh, V. and Iqbal, S. S., (2022). Urban Flood Susceptibility Zonation Mapping Using Evidential Belief Function, Frequency Ratio and Fuzzy Gamma Operator Models in GIS: A Case Study of Greater Mumbai, Maharashtra, India. *Geocarto International*, Vol. 37(2), 581–606. https://doi.org/10.1080/10106049.2020.1730448.

[22] Mehravar, S., Razavi-Termeh, S. V., Moghimi, A., Ranjgar, B., Foroughnia, F. and Amani, M., (2023). Flood Susceptibility Mapping Using Multi-Temporal SAR Imagery and Novel Integration of Nature-Inspired Algorithms into Support Vector Regression. *Journal of Hydrology (Amst)*, Vol. 617. https://doi.org/10.1016/j.jhydrol.2023.129100.

[23] Arabameri, A., Danesh, A. S., Santosh, M., Cerda, A., Pal, S. C., Ghorbanzadeh, O., Roy, P. and Chowdhuri, I., (2022). Flood Susceptibility Mapping Using Meta-Heuristic Algorithms. *Geomatics, Natural Hazards and Risk*, Vol. 13(1), 949–974. https://doi.org/10.1080/19475705.2022.2060138.

[24] Pourghasemi, H. R., Razavi-Termeh, S. V., Kariminejad, N., Hong, H. and Chen, W., (2020). An Assessment of Metaheuristic Approaches for Flood Assessment. *Journal of Hydrology (Amst)*, Vol. 582. https://doi.org/10.1016/j.jhydrol.2019.124536.

[25] Nachappa, T. G., Tavakkoli Piralilou, S., Gholamnia, K., Ghorbanzadeh, O., Rahmati, O. and Blaschke, T., (2020). Flood Susceptibility Mapping with Machine Learning, Multi-Criteria Decision Analysis and Ensemble Using Dempster Shafer Theory. *Journal of Hydrology (Amst)*, Vol. 590. https://doi.org/10.1016/j.jhydrol.2020.125275.

[26] Loi, D., (2023). Assessment of Urban Flood Vulnerability Using Integrated Multi-parametric AHP and GIS. *International Journal of Geoinformatics*, Vol. 19(6), 1–16. https://doi.org/10.52939/ijg.v19i6.2689.

[27] Choubin, B., Moradi, E., Golshan, M., Adamowski, J., Sajedi-Hosseini, F. and Mosavi, A., (2019). An Ensemble Prediction of Flood Susceptibility Using Multivariate Discriminant Analysis, Classification and Regression Trees, and Support Vector Machines. *Science of the Total Environment*, Vol. 651, 2087–2096. https://doi.org/10.1016/j.scitotenv.2018.10.064.

[28] Chowdhuri, I., Pal, S. C. and Chakrabortty, R., (2020). Flood Susceptibility Mapping by Ensemble Evidential Belief Function and Binomial Logistic Regression Model on River Basin of Eastern India. *Advances in Space Research*, Vol. 65(5), 1466–1489. https://doi.org /10.1016/j.asr.2019.12.003.

[29] Park, N. W., (2011). Application of Dempster-Shafer Theory of Evidence to GIS-based Landslide Susceptibility Analysis. *Environmental Earth Sciences*, Vol. 62(2), 367–376. https://doi.org/10.1007/s12665-010-0531-5.

[30] Shafer, G., (2016). A Mathematical Theory of Evidence Turns 40. *International Journal of Approximate Reasoning*, Vol. 79, 7–25. https://doi.org/10.1016/j.ijar.2016.07.009.

[31] Bhardwaj, S. and Veerappan, R., (2023). Flood Susceptibility Zonation Using Dempster-Shafer Evidential Belief Function (EBF) Method in Chalakudy Taluk, Kerala, India. *Impacts of Urbanization on Hydrological Systems in India*, Thambidurai, P. and Dikshit, A. K. (Eds.,) Cham: Springer International Publishing. 79–109. https://doi.org/10.1007/978-3-031-21618-35.

[32] Tehrany, M. S. and Kumar, L., (2018). The Application of a Dempster–Shafer-based Evidential Belief Function in Flood Susceptibility Mapping and Comparison with Frequency Ratio and Logistic Regression Methods. *Environmental Earth Sciences*, Vol. 77(13). https://doi.org/10.1007/s12665-018-7667-0.

[33] Kaya, C. M. and Derin, L., (2023). Parameters and Methods Used in Flood Susceptibility Mapping: A Review. *Journal of Water and Climate Change*, Vol. 14(6), 1935–1960. https://doi.org/10.2166/wcc.2023.035.

[34] Pontius, R. G. and Parmentier, B., (2014). Recommendations for Using the Relative Operating Characteristic (ROC). *Landscape Ecology*, Vol. 29(3), 367–382. https://doi.org/10.1007/s10980-013-9984-8.

[35] Arabameri, A., Saha, S., Chen, W., Roy, J., Pradhan, B. and Bui, D. T., (2020). Flash Flood Susceptibility Modelling Using Functional Tree and Hybrid Ensemble Techniques. *Journal of Hydrology (Amst)*, Vol. 587. https://doi.org/10.1016/j.jhydrol.2020.125007.

[36] Termeh, R. S. V., Kornejady, A., Pourghasemi, H. R. and Keesstra, S., (2018). Flood Susceptibility Mapping Using Novel Ensembles of Adaptive Neuro Fuzzy Inference System and Metaheuristic Algorithms. *Science of The Total Environment*, Vol. 615, 438–451. https://doi.org/10.1016/j.scitotenv.2017.09.262

[37] Al-Abadi, A. M., (2018). Mapping Flood Susceptibility in an Arid Region of Southern Iraq Using Ensemble Machine Learning Classifiers: A Comparative Study. *Arabian Journal of Geosciences*, Vol. 11(9). https://doi.org/10.1007/s12517-018-3584-5.

[38] Ullah, K. and Zhang, J., (2020). GIS-based Flood Hazard Mapping Using Relative Frequency Ratio Method: A Case Study of Panjkora River Basin, Eastern Hindu Kush, Pakistan. *PLoS One*, Vol. 15(3). https://doi.org/10.1371/journal.pone.0229153.

[39] Islam, A. R. M. T., Talukdar, S., Mahato, S., Kundu, S., Eibek, K. U., Pham, Q. B., Kuriqu, A. and Linh, N. T. T., (2021). Flood Susceptibility Modelling Using Advanced Ensemble Machine Learning Models. *Geoscience Frontiers*, Vol. 12(3). https://doi.org/10.1016/j.gsf.2020.09.006.

[40] Avand, M., Kuriqi, A., Khazaei, M. and Ghorbanzadeh, O., (2022). DEM Resolution Effects on Machine Learning Performance for Flood Probability Mapping. *Journal of Hydro-environment Research*, Vol. 40(1), 1–16. https://doi.org/10.1016/j.jher.2021.10.002.

[41] Ghosh, B., (2023). Flood Susceptibility Assessment and Mapping in a Monsoon-Dominated Tropical River Basin Using GIS-based Data-Driven Bivariate and Multivariate Statistical Models and their Ensemble Techniques. *Environmental Earth Sciences*, Vol. 82(1). https://doi.org/10.1007/s12665-022-10696-z.

[42] Nguyen, D., Chou, T., Hoang, T., and Chen, M. (2023). Flood Susceptibility Mapping Using Machine Learning Algorithms: A Case Study in Huong Khe District, Ha Tinh Province, Vietnam. *International Journal of Geoinformatics*, Vol. 19(7), 1–15. https://doi.org/10.52939/ijg.v19i7.2739.

[43] Zevenbergen, L. W. and Thorne, C. R., (1987). Quantitative Analysis of Land Surface Topography. *Earth Surface Processes and Landforms*, Vol. 12(1), 47–56. https://doi.org/10.1002/esp.3290120107.

[44] Tehrany, M. S., Pradhan, B., Mansor, S. and Ahmad, N., (2015). Flood Susceptibility Assessment Using GIS-based Support Vector Machine Model with Different Kernel Types. *Catena*, Vol. 125, 91–101. https://doi.org/10.1016/j.catena.2014.10.017

[45] Moore, I. D., Grayson, R. B. and Ladson, A. R., (1991). Digital Terrain Modelling: A Review of Hydrological, Geomorphological, and Biological Applications. *Hydrological Processes*, Vol. 5(1), 3–30. https://doi.org/10.1002/hyp.3360050103.

[46] Mohd Rasu, M., Suhandri, H., Khalifa, N., Abdul Rasam, A., and Hamid, A. (2023). Evaluation of Flood Risk Map Development through GIS-Based Multi-Criteria Decision Analysis in Maran District, Pahang - Malaysia. *International Journal of Geoinformatics*, Vol. 19(10), 1–16. https://doi.org/10.52939/ijg.v19i9.2873

[47] Strahler, A. N., (1952). Hypsometric (Area-Altitude) Analysis of Erosional Topography. *GSA Bulletin*, Vol. 63(11), 1117–1142. https://doi.org/10.1130/0016-7606(1952)63[1117:HAAOET]2.0.CO;2.

[48] Wang, Y., Hong, H., Chen, W., Li, S., Panahi, M., Khosravi, K., Shirzadi, A., Shahabi, H., Panahi, S. and Costache, R., (2019). Flood Susceptibility Mapping in Dingnan County (China) Using Adaptive Neuro-Fuzzy Inference System with Biogeography Based Optimization and Imperialistic Competitive Algorithm. *Journal of Environmental Management*, Vol. 247, 712–729. https://doi.org/10.1016/j.jenvman.2019.06.102.

[49] Rahmati, O., Pourghasemi, H. R. and Zeinivand, H., (2016). Flood Susceptibility Mapping Using Frequency Ratio and Weights-Of-Evidence Models in the Golastan Province, Iran. *Geocarto International*, Vol. 31(1), 42–70. https://doi.org/10.1080/10106049.2015.1041559.

[50] Ozegin, K. O. and Ilugbo, S. O., (2024). Evaluation of Potentially Susceptible Flooding Areas Leveraging Geospatial Technology with Multicriteria Decision Analysis in Edo State, Nigeria. *Natural Hazards Research*, In Press. https://doi.org/10.1016/j.nhres.2024.07.002.

[51] Khosravi, K., Pham, B. T., Chapi, K., Shirzadi, A., Shahabi, H., Revhaug, I., Prakash, I. and Bui, D. T., (2018). A Comparative Assessment of Decision Trees Algorithms for Flash Flood Susceptibility Modeling at Haraz Watershed, Northern Iran. *Science of The Total Environment*, Vol. 627, 744–755. https://doi.org/10.1016/j.scitotenv.2018.01.266.

[52] Pradhan, B., Lee, S., Dikshit, A. and Kim, H., (2023). Spatial Flood Susceptibility Mapping Using an Explainable Artificial Intelligence (XAI) Model. *Geoscience Frontiers*, Vol. 14(6). https://doi.org/10.1016/j.gsf.2023.101625.

[53] Pourghasemi, H. R., Moradi, H. R. and Aghda, S. M. F., (2013). Landslide Susceptibility Mapping by Binary Logistic Regression, Analytical Hierarchy Process, And Statistical Index Models and Assessment of their Performances. *Natural Hazards*, Vol. 69(1), 749–779. https://doi.org/10.1007/s11069-013-0728-5.

[54] O'brien, R. M., (2007). A Caution Regarding Rules of Thumb for Variance Inflation Factors. *Qual Quant*, Vol. 41(5), 673-690. https://doi.org/10.1007/s11135-006-9018-6.

[55] Hair, J. F., Black, W. C., Babin, B. J. and Anderson, R. E., (2010) *Multivariate Data Analysis*. 7th Edition. Prentice Hall.

[56] Roy, D., Sarkar, A., Kundu, P., Paul, S. and Sarkar, B, C., (2023). An Ensemble of Evidence Belief Function (EBF) with Frequency Ratio (FR) Using Geospatial Data for Landslide Prediction in Darjeeling Himalayan Region of India. *Quaternary Science Advances*, Vol. 11. https://doi.org/10.1016/j.qsa.2023.100092.

[57] Dempster, A. P., (1968). A Generalization of Bayesian Inference. *Journal of the Royal Statistical Society. Series B (Methodological)*, Vol. 30(2), 205–247.

[58] Shafer, G., (1976). *A Mathematical Theory of Evidence*. Princeton University Press. https://doi.org/10.2307/j.ctv10vm1qb.

[59] Liu, J. G. and Mason, P. J., (2009). *Essential Image Processing and GIS for Remote Sensing*. John Wiley & Sons.

[60] Wright, D. F. and Bonham-Carter, G., (1996). VHMS Favourability Mapping with GIS-based Integration Models, Chisel Lake-Anderson Lake Area. https://doi.org/10.4095/207595.

[61] Paul, G. C., Saha, S. and Hembram, T. K., (2019). Application of the GIS-Based Probabilistic Models for Mapping the Flood Susceptibility in Bansloi Sub-basin of Ganga-Bhagirathi River and their Comparison. *Remote Sensing in Earth Systems Sciences*, Vol. 2(2), 120–146. https://doi.org/10.1007/s41976-019-00018-6.

[62] Nykänen, V., Lahti, I., Niiranen, T. and Korhonen, K., (2015). Receiver Operating Characteristics (ROC) as Validation Tool for Prospectivity Models-A Magmatic Ni–Cu Case Study from the Central Lapland Greenstone Belt, Northern Finland. *Ore Geology Reviews*, Vol. 71, 853–860. https://doi.org/10.1016/j.oregeorev.2014.09.007.

[63] Arabameri, A., Rezaei, K., Cerdà, A., Conoscenti, C. and Kalantari, Z., (2019). A Comparison of Statistical Methods and Multi-Criteria Decision Making to Map Flood Hazard Susceptibility in Northern Iran. *Science of The Total Environment*, Vol. 660, 443–458. https://doi.org/10.1016/j.scitotenv.2019.01.021

[64] Nachappa, G. T. and Meena, S. R., (2020). A Novel Per Pixel and Object-Based Ensemble Approach for Flood Susceptibility Mapping. *Geomatics, Natural Hazards and Risk*, Vol. 11(1), 2147–2175. https://doi.org/10.1080/19475705.2020.1833990.